Topological Insulator Thin Films of Bi_2Te_3 with Controlled Electronic Structure

Guang Wang, Xie-Gang Zhu, Yi-Yang Sun, Yao-Yi Li, Tong Zhang, Jing Wen, Xi Chen, Ke He, Li-Li Wang, Xu-Cun Ma, Jin-Feng Jia, Shengbai B. Zhang, and Qi-Kun Xue**

Bismuth-based binary compounds such as Bi_2Te_3 and Bi_2Se_3 have been known for a long time to be excellent thermoelectric materials due to their unique near-gap electronic structure.[1–6] Recently, it was shown that these materials host novel topological surface states inside the bulk energy gaps that are protected by the time reversal symmetry. The topological surface states exhibit a variety of exotic electromagnetic phenomena such as Majorana fermions[7] and magnetic monopoles[8] and have attracted considerable attention in material sciences and condensed matter physics.[9–23] The electronic properties of bulk Bi_2Te_3 and Bi_2Se_3 crystals are usually dominated by electron donors, resulting in n-type conductivity.[11–13,24,25] When the donors dominate, the Dirac point is buried deep below the Fermi level, which makes it difficult to characterize the topological transport properties and to develop topological devices that rely on the behavior of surface Dirac fermions. To compensate for the unintentional donors, a high-concentration of extrinsic dopants, for example, more than 0.67% Sn[11] or 1% Cd,[20] has been introduced into Bi_2Te_3. With a substitution of Bi by 1% Ca, p-type $Bi_{1.98}Ca_{0.02}Se_3$ has also been reported.[13] Such a high dopant concentration, however, can affect the carrier transport considerably through undesirable impurity scattering. Growing high-quality topological insulator materials with controllable electronic structures has become one of the most critical issues in the rapidly developing field of topological insulators.

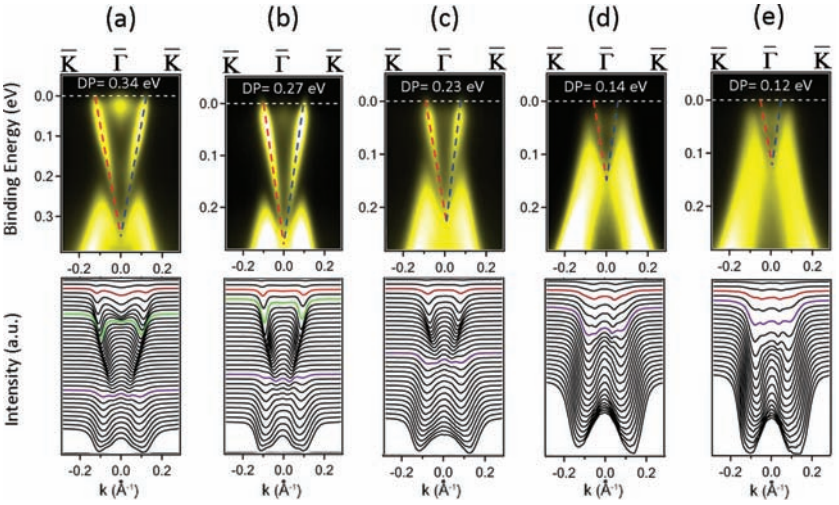

Figure 1. $\overline{\Gamma}-\overline{K}$ band structure evolution with T_{Si}: a) 560 K (DP = 0.34 eV), b) 580 K (DP = 0.27 eV), c) 600 K (DP = 0.23 eV), d) 625 K (DP = 0.14 eV), and e) 630 K (DP = 0.12 eV). Upper panels show the ARPES intensity maps and lower panels show the corresponding MDC, measured at an interval of 10 meV. Red, purple, and green curves mark E_F, VBM, and conduction band minimum (CBM), respectively.

In this work, we demonstrate that high-quality insulating and p-type Bi_2Te_3 thin films can be grown by regulating the growth kinetics during molecular beam epitaxy (MBE) without any extrinsic doping. As revealed by the angle-resolved photoemission spectroscopy (ARPES), the Fermi energy (E_F) of the Bi_2Te_3 films can be tuned with the Si substrate temperature (T_{Si}) for a given Te_2/Bi beam flux ratio (θ). A conversion from n- to p-type is observed and correlated with a change in the growth mode from layer-by-layer to step-flow. Using a combined study of the scanning tunneling microscopy/spectroscopy (STM/STS) and first-principles calculations, we identify the defects responsible for the donor and acceptor states as the Te-on-Bi and Bi-on-Te antisites, respectively. From the STM images, we estimate that the concentration of the acceptor defects is 0.02%, which is about two orders of magnitude smaller than what is required by extrinsic doping. This suggests that the concentrations of unintentional donors in our samples are also orders of magnitude smaller than those in conventional Bi_2Te_3. Such high-quality Bi_2Te_3 thin films with tunable conduction type enable the study of intrinsic topological properties without the obstruction and interference by a high density of dopants and allow for more flexible designs of topological devices based on this material.

Figure 1 shows a set of ARPES spectra, which reveal that E_F moves systematically with T_{Si}. In particular, at an optimal θ = 18, the sample grown at 560 K (Figure 1a) exhibits a Dirac point (DP) at binding energy (E_B) = 0.34 eV, while its E_F is in the

G. Wang, X.-G. Zhu, Y.-Y. Li, J. Wen, Prof. X. Chen, Prof. J.-F. Jia, Prof. Q.-K. Xue
State Key Lab of Low Dimensional Quantum Physics
Department of Physics
Tsinghua University
Beijing 100084, P. R. China
E-mail: qkxue@mail.tsinghua.edu.cn
Dr. Y.-Y. Sun, Prof. S. B. Zhang
Department of Physics
Applied Physics, and Astronomy
Rensselaer Polytechnic Institute
Troy, New York 12180, USA
E-mail: zhangs9@rpi.edu
Dr. T. Zhang, Dr. K. He, Dr. L.-L. Wang, Prof. X.-C. Ma, Prof. Q.-K. Xue
Institute of Physics
The Chinese Academy of Sciences
Beijing 100190, P. R. China

DOI: 10.1002/adma.201100678

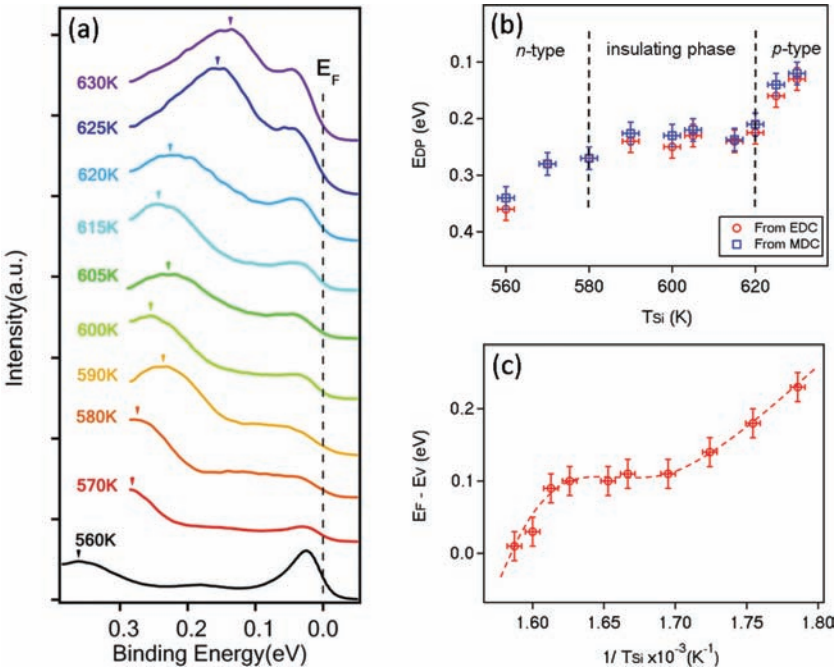

Figure 2. a) Normal emission ARPES spectra at different growth Si substrate temperatures (T_{Si}). Ticks mark the Dirac points (E_{DP}). b) The E_{DP} evolution showing the n-type to p-type conversion. c) The dependence of the relative E_F positions on the reciprocal of substrate temperature ($1/T_{Si}$). The dashed line is a guide for the eye.

conduction band. Here, the bulk states are seen as an intense spot right below the E_F. The sample is thus n-type. When increasing T_{Si} to 580 K and 600 K, the DPs increase to $E_B = 0.27$ and 0.23 eV, respectively (see Figure 1b,c). In both cases, the E_F resides inside the bulk gap, thereby realizing the insulating phase. When T_{Si} exceeds 620 K, the Bi_2Te_3 sample turns into p-type, with its E_F close to the valence band. The DPs for samples grown at 625 and 630 K are at $E_B = 0.14$ eV (Figure 1d) and 0.12 eV (Figure 1e), respectively. The above trend can be more clearly seen in the momentum distribution curves (MDC) in the lower panels of Figure 1, where the distance between E_F (red) and the valence band maximum (VBM) (purple) decreases as T_{Si} increases.

Figure 2a shows a series of normal emission spectra of Bi_2Te_3 as a function of T_{Si}. Peaks marked by the arrows indicate the positions of the DP, which has a trend very similar to that in Figure 1; this can be seen in Figure 2b where the DPs taken from both the MDC (Figure 1) and the energy distribution curve (EDC) (Figure 2a) are compared. Figure 2b can be separated into three parts for n-type, insulating, and p-type phases. It also suggests that the critical T_{Si}, at which the n- to p-type conversion takes place, is about 620 K. This critical T_{Si} may change due to different θ, but the general trend demonstrated in Figure 2b does not change.

The conversion in the conduction type was found to be accompanied by a change in the growth mode. **Figure 3**a shows a real-time evolution of the reflection high energy electron diffraction (RHEED) intensity for a (0,0) diffraction peak during deposition at different T_{Si}. An intensity oscillation (red curves in Figure 3a) was observed when T_{Si} was below 620 K, which is characteristic of a layer-by-layer growth.[18] Deposition at higher T_{Si} leads to a featureless RHEED intensity (black curves in Figure 3a), which is characteristic of a step-flow growth.[26]

Based on the sample preparation conditions, we believe intrinsic defects are responsible for the observed type conversion. Figure 3b,c show the STM images for an n-type ($T_{Si} = 590$ K) and a p-type ($T_{Si} = 630$ K) film. Two typical types of defects are commonly observed in these films: one has a triangular depression (TD), whereas the other has a clover-shaped protrusion (CSP). These defects can be more clearly identified in the high-resolution STM image in Figure 3d. There are also bright spots above some of the TDs or CSPs in the low-temperature samples in Figure 3b, but not in the high-temperature samples (see discussion below). In the filled-state topographic image, the CSP defect is characterized by an enhanced intensity surrounding the defect, implying that the defect is negatively charged. In other words, it is an acceptor. The dI/dV plot in Figure 3e identifies a defect state at a negative bias of –0.3 V for the same defect. As for the TD defect, on the other hand,

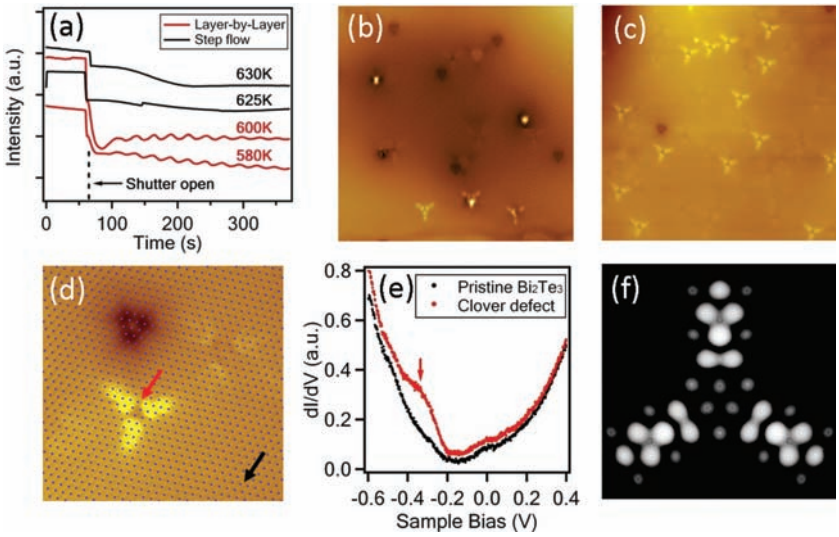

Figure 3. a) Growth temperature dependence of RHEED intensity of the (0,0) diffraction versus growth time. b,c) STM images (50 nm × 50 nm, $V_B = -0.6$ V) for layer-by-layer and step-flow grown samples, respectively. d) High-resolution zoomed-in STM image (13 nm × 13 nm, $V_B = -0.4$ V) for the two kinds of defects in (c). e) Spatially averaged dI/dV measurements indicating the energy position of the clover-shaped defect in (d). f) Simulated STM image for a Bi_{Te} antisite at the fifth layer.

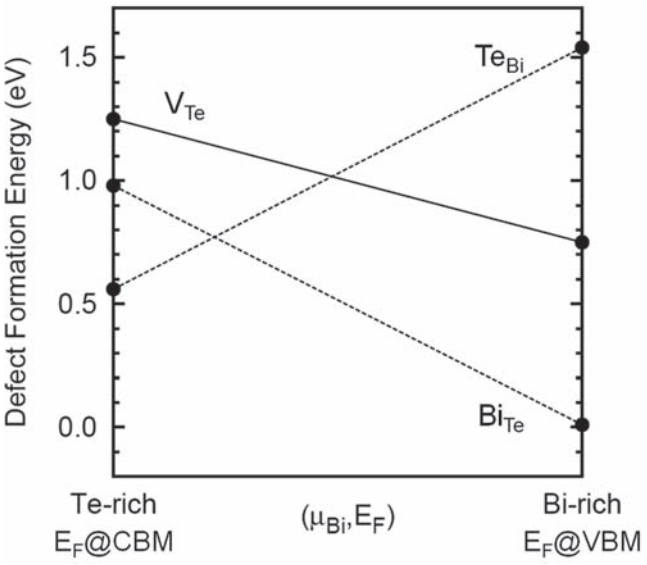

Figure 4. Calculated formation energies for Bi_{Te}^{-}, Te_{Bi}^{+}, and V_{Te}^{0}, as a function of (μ_{Bi}, E_F). The Te-rich and Bi-rich conditions correspond to μ_{Te} and μ_{Bi} being equal to those of bulk Te and Bi, respectively. Also, at equilibrium with bulk Bi_2Te_3, μ_{Te} and μ_{Bi} satisfy $2\mu_{Bi} + 3\mu_{Te} = E(Bi_2Te_3)$, the total energy of bulk Bi_2Te_3 per formula. Data for V_{Te}^{0} are exact. For antisites, the dashed lines are used to guide the eyes, and the actual curves joining the end points may not be linear.

the depressed region surrounding the defect suggests that it should be a donor.

First-principles density functional calculations were carried out to establish the atomic origin for the observed defects. **Figure 4** shows the calculated formation energy (E_{form}) for three low-energy native defects as a function of the Bi chemical potential μ_{Bi}: a low μ_{Bi} corresponds to the Te-rich growth condition, whereas a high μ_{Bi} corresponds to the Bi-rich growth condition. We find that the Bi-on-Te antisite defect (Bi_{Te}) is an acceptor, whereas the Te-on-Bi antisite defect (Te_{Bi}) is a donor. The apparent triangular depression of the TD defect in the STM image in Figure 3d suggests that this defect could be a vacancy such as Te vacancy (V_{Te}). However, our calculation shows that V_{Te} is charge neutral and cannot be a donor. Thus, we assign the TD defect to Te_{Bi} antisite, which also has low formation energy under the Te-rich conditions (see Figure 4). We can also assign the CSP defect to Bi_{Te} antisite. On a first look, it is unclear why the Bi_{Te} antisite should have such a large spatial distribution, as revealed in Figure 3d. Our first-principles calculations suggest that the Bi_{Te} is not in the surface layer but in the fifth layer of the first quintuple layer (QL). The simulated STM image for Bi_{Te} in Figure 3f is indeed in good agreement with experiment. Regarding the bright spots in the low-growth temperature n-type samples mentioned earlier, we believe they are not a completely new defect but a Te adatom bound to a second layer Te_{Bi} or attracted to a surface Te above the fifth layer Bi_{Te}. Thus, the formation of the Bi_{Te} acceptor at higher growth temperature is the reason for the n- to p-type conversion.

The areal CSP defect density in our p-type samples, as revealed by the STM, is about 6×10^{11} cm^{-2}. The results presented above show that these are the subsurface defects within a QL of about 1.0 nm thickness. Therefore, we estimate the density of Bi_{Te} acceptors to be 6×10^{11} cm^{-2} per 1.0 nm, i.e., 6×10^{18} cm^{-3}. This can be compared with the atomic density of Bi_2Te_3 to be about 3×10^{22} cm^{-3}. Hence, the concentration of the intrinsic acceptors in The p-type samples is only 0.02%, which is about two orders of magnitude smaller than that required by extrinsic doping.

The key element that controls the type conversion is the surface Te coverage during the MBE growth. Although we have a nominal θ close to 20, the sample may not always be as Te rich: at low enough growth temperature, we can expect the sample to be Te rich. The bright spots in Figure 3b are evidence for the excess of Te; they are the Te adatoms bound to the Te that is already incorporated into the surface or subsurface layers. At higher growth temperatures, the excess Te will diffuse on the surface and eventually desorb as Te_2 gas molecules. This explains why the bright spots are only seen at low growth temperature. It may also signal that a transition from Te rich towards Te poor (or Bi rich) has taken place at these temperatures. The surface diffusion of the deposited Te and Bi is a necessary condition for the step-flow growth. The diffusion of Bi is also a necessary condition for the Bi to fill in the vacant sites left by the Te_2 desorption, resulting in more Bi_{Te} antisites. These kinetic arguments qualitatively explain why the change in growth mode from layer-by-layer to step-flow coincides with the n- to p-type conversion.

There is also a thermodynamic reason for the conduction type conversion. Figure 4 shows that under the Te-rich conditions the formation energy of Te_{Bi} is 0.56 eV for E_F at the conduction band minimum (CBM), whereas the formation energy of Bi_{Te} is 0.98 eV under the same conditions. Hence, the Te_{Bi} donor is the main defect in the Te-rich samples, giving rise to n-type conduction. Under the Bi-rich conditions, on the other hand, the formation energy of Bi_{Te} is slightly positive for E_F at the VBM, whereas the formation energy of Te_{Bi} is 1.54 eV under the same conditions. Hence, the Bi_{Te} acceptor becomes the main defect in the Bi-rich samples, giving rise to the conversion to p-type.

Finally, it is tempting to comment on the inverse growth temperature dependence of E_F relative to the VBM (E_V) in Figure 2c, which is taken from the MDC data in Figure 2b. In the high-temperature regime, the change in $E_F - E_V$ is approximately proportional to that in $1/T_{Si}$. This is because 1) the hole concentration in the p-type sample is given[27] by $p = N_{eff}^{v} \exp\left[-\frac{E_F - E_V}{kT_m}\right]$, where N_{eff}^{v} is the effective density of states at the VBM, k is the Boltzmann constant, and T_m is the measurement temperature, and 2) the equilibrium concentration of the acceptors (C_A) can be described[28] by $C_A = N_S \exp\left[-\frac{E_{form}}{kT_{Si}}\right]$, where E_{form} is the acceptor formation energy and N_S is the concentration of all possible lattice sites for the defect. Holes in the p-type samples are primarily from acceptors and hence $p \approx C_A$. This implies that $E_F - E_V \propto 1/T_{Si}$. In the intermediate-temperature regime, the formation of donors competes with the formation of acceptors and the two compensate each other, resulting in relatively flat $1/T_{Si}$ dependence. In the low-temperature regime, the donor is dominant. However, as we have mentioned earlier, its concentration is determined by the kinetics of the Te adsorption rather than the defect energetics.

In summary, using a joint ARPES/STM experimental and first-principles theoretical study, we demonstrate that the electronic properties of the Bi_2Te_3 thin films can be regulated by altering the MBE growth conditions without extrinsic dopants. A conversion from n- to p-type conduction in the Bi_2Te_3 thin films is observed when the Si substrate temperature is increased above a critical temperature. The type conversion is found accompanied by a change in the growth mode from layer-by-layer to step-flow. First-principles calculations suggest that the type conversion is a result of the change in the concentrations of Te_{Bi} antisite donors and Bi_{Te} antisite acceptors due to growth condition changes. By achieving orders of magnitude smaller defect density and more controllable conduction-type conversion than what is currently available by extrinsic doping, our finding represents a solid step forward in preparing and controlling intrinsic topological surface states for their salient physical properties as well as for potential applications.

Experimental Section

Experimental Details: The experiments were carried out in an ultrahigh vacuum system consisting of an MBE growth chamber, a low temperature STM (Omicron), and an ARPES apparatus (Gammadata Scienta). The Bi_2Te_3 films were grown on the Si(111)-7 × 7 substrate with high purity of Bi (99.9999%) and Te (99.999%) by MBE, with a fixed nominal θ around 20. Defining T_{Bi}, T_{Si}, and T_{Te} as the Bi-cell, Si-substrate, and Te-cell temperatures, respectively, the optimal growth condition was previously found to be $T_{Bi} > T_{Si} > T_{Te}$.[18,19] At T_{Bi} = 823 K, T_{Te} = 583 K, and T_{Si} = 600 K, the typical growth rate is about 2.2 QL per minute. All the films studied in this work have a thickness of 60 QL. To carry out ARPES measurements, photoelectrons were excited by the He-Iα resonant line (21.21 eV) and collected using a Scienta R4000 analyzer. The STM images were acquired using chemically etched polycrystalline tungsten tips. The ARPES and STM data were acquired at 77 K. All the ARPES spectra were acquired within 30 min after the preparation of the films.

First-Principles Calculations: The calculations were based on density-functional theory, as implemented in the Vienna Ab-initio Simulation Package.[29] The generalized gradient approximation of Perdew, Burke, and Ernzerhof[30] was used for the exchange-correlation functional. Core-electrons were represented by the projector augmented wave potentials.[31] Plane waves with a cutoff energy of 250 eV were used as the basis set. A (4 × 4 × 1) 240-atom supercell was used in the defect calculations. A single special k-point at (7/24, 1/12, 1/4) was used to sample the Brillouin zone. Defect formation energies were calculated following the formalism in Ref. [28]. An STM image of the Bi_{Te} defect was simulated using a (10 × 10) surface supercell with a single quintuple layer.

Acknowledgements

Work in Beijing was supported by the National Science Foundation and Ministry of Science & Technology of China. Work at RPI was supported by the US Department of Energy under Grant No. DE-SC0002623. Supercomputer time was provided by the CCNI at RPI and the NSF TeraGrid at TACC under Grant No. TG-DMR100014.

Received: February 19, 2011
Published online:

[1] G. A. Thomas, D. H. Rapkine, R. B. Van Dover, L. F. Mattheiss, W. A. Sunder, L. F. Schneemeyer, J. V. Waszczak, *Phys. Rev. B* **1992**, *46*, 1553.
[2] S. K. Mishra, S. Satpathy, O. Jepsen, *J. Phys.: Condens. Matter* **1997**, *9*, 461.
[3] P. Larson, S. D. Mahanti, M. G. Kanatzidis, *Phys. Rev. B* **2000**, *61*, 8162.
[4] S. J. Youn, A. J. Freeman, *Phys. Rev. B* **2001**, *63*, 085112.
[5] S. Urazhdin, D. Bilc, S. H. Tessmer, S. D. Mahanti, Theodora Kyratsi, M. G. Kanatzidis, *Phys. Rev. B* **2002**, *66*, 161306.
[6] S. Urazhdin, D. Bilc, S. D. Mahanti, S. H. Tessmer, Theodora Kyratsi, M. G. Kanatzidis, *Phys. Rev. B* **2004**, *69*, 085313.
[7] L. Fu, C. L. Kane, *Phys. Rev. Lett.* **2008**, *100*, 096407.
[8] X.-L. Qi, R. D. Li, J. D. Zang, S.-C. Zhang, *Science* **2009**, *323*, 1184.
[9] H. J. Zhang, C.-X. Liu, X.-L. Qi, X. Dai, Z. Fang, S.-C. Zhang, *Nat. Phys.* **2009**, *5*, 438.
[10] Y. Xia, D. Qian, D. Hsieh, L. Wray, A. Pal, H. Lin, A. Bansil, D. Grauer, Y. S. Hor, R. J. Cava, M. Z. Hasan, *Nat. Phys.* **2009**, *5*, 398.
[11] Y. L. Chen, J. G. Analytis, J.-H. Chu, Z. K. Liu, S.-K. Mo, X.-L. Qi, H. J. Zhang, D. H. Lu, X. Dai, Z. Fang, S.-C. Zhang, I. R. Fisher, Z. Hussain, Z.-X. Shen, *Science* **2009**, *325*, 178.
[12] D. Hsieh, Y. Xia, D. Qian, L. Wray, J. H. Dil, F. Meier, J. Osterwalder, L. Patthey, J. G. Checkelsky, N. P. Ong, A. V. Fedorov, H. Lin, A. Bansil, D. Grauer, Y. S. Hor, R. J. Cava, M. Z. Hasan, *Nature* **2009**, *460*, 1101.
[13] Y. S. Hor, A. Richardella, P. Roushan, Y. Xia, J. G. Checkelsky, A. Yazdani, M. Z. Hasan, N. P. Ong, R. J. Cava, *Phys. Rev. B* **2009**, *79*, 195208.
[14] D. Hsieh, Y. Xia, D. Qian, L. Wray, F. Meier, J. H. Dil, J. Osterwalder, L. Patthey, A. V. Fedorov, H. Lin, A. Bansil, D. Grauer, Y. S. Hor, R. J. Cava, M. Z. Hasan, *Phys. Rev. Lett.* **2009**, *103*, 146401.
[15] Y. Xia, D. Qian, D. Hsieh, R. Shankar, H. Lin, A. Bansil, A. V. Fedorov, D. Grauer, Y. S. Hor, R. J. Cava, M. Z. Hasan, arXiv:0907.3089v1 [cond-mat.mes-hall].
[16] G. H. Zhang, H. J. Qin, J. Teng, J. D. Guo, Q. L. Guo, X. Dai, Z. Fang, K. H. Wu, *Appl. Phys. Lett.* **2009**, *95*, 053114.
[17] Y. Zhang, K. He, C.-Z. Chang, C.-L. Song, L.-L. Wang, X. Chen, J.-F. Jia, Z. Fang, X. Dai, W.-Y. Shan, S.-Q. Shen, Q. Niu, X.-L. Qi, S.-C. Zhang, X.-C. Ma, Q.-K. Xue, *Nat. Phys.* **2010**, *6*, 584.
[18] Y.-Y. Li, G. Wang, X.-G. Zhu, M.-H. Liu, C. Ye, X. Chen, Y.-Y. Wang, K. He, L.-L. Wang, X.-C. Ma, H.-J. Zhang, X. Dai, Z. Fang, X.-C. Xie, Y. Liu, X.-L. Qi, J.-F. Jia, S.-C. Zhang, Q.-K. Xue, *Adv. Mater.* **2010**, *22*, 4002.
[19] T. Zhang, P. Cheng, X. Chen, J.-F. Jia, X. C. Ma, K. He, L. L. Wang, H. J. Zhang, X. Dai, Z. Fang, X. C. Xie, Q.-K. Xue, *Phys. Rev. Lett.* **2009**, *103*, 266803.
[20] Z. Alpichshev, J. G. Analytis, J.-H. Chu, I. R. Fisher, Y. L. Chen, Z. X. Shen, A. Fang, A. Kapitulnik, *Phys. Rev. Lett.* **2010**, *104*, 016401.
[21] P. Cheng, C. L. Song, T. Zhang, Y. Y. Zhang, Y. L. Wang, J.-F. Jia, J. Wang, Y. Y. Wang, B. F. Zhu, X. Chen, X. C. Ma, K. He, L. L. Wang, X. Dai, Z. Fang, X. C. Xie, X.-L. Qi, C.-X. Liu, S.-C. Zhang, Q.-K. Xue, *Phys. Rev. Lett.* **2010**, *105*, 076801.
[22] X.-L. Qi, S.-C. Zhang, *Phys. Today* **2010**, *63*, 33.
[23] M. Z. Hasan, C. L. Kane, *Rev. Mod. Phys.* **2010**, *82*, 3045.
[24] S. Cho, Y. Kim, A. DiVenere, G. K. Wong, J. B. Ketterson, J. R. Meyer, *Appl. Phys. Lett.* **1999**, *75*, 1401.
[25] J. Kašparová, Č. Drašar, A. Krejčová, L. Beneš, P. Lošťák, Wei Chen, Zhenhua Zhou, C. Uher, *J. Appl. Phys.* **2005**, *97*, 103720.
[26] T. Nishinaga, *Prog. Cryst. Growth Ch.* **2004**, *48/49*, 104.
[27] H. Ibach, H. Lüth, *Solid-State Physics*, Springer, Berlin, **1995**.
[28] S. B. Zhang, J. E. Northrup, *Phys. Rev. Lett.* **1991**, *67*, 2339.
[29] G. Kresse, J. Furthmüller, *Comput. Mater. Sci.* **1996**, *6*, 15.
[30] J. P. Perdew, K. Burke, M. Ernzerhof, *Phys. Rev. Lett.* **1996**, *77*, 3865.
[31] G. Kresse, D. Joubert, *Phys. Rev. B* **1999**, *59*, 1758.